Microwave Energy Drives "On–Off–On" Spin-Switch Behavior in Nitrogen-Doped Graphene

Giorgio Zoppellaro,* Aristides Bakandritsos, Jiří Tuček, Piotr Błoński, Toma Susi, Petr Lazar, Zdeněk Baďura, Tomáš Steklý, Ariana Opletalová, Michal Otyepka, and Radek Zbořil*

The established application of graphene in organic/inorganic spin-valve spintronic assemblies is as a spin-transport channel for spin-polarized electrons injected from ferromagnetic substrates. To generate and control spin injection without such substrates, the graphene backbone must be imprinted with spin-polarized states and itinerant-like spins. Computations suggest that such states should emerge in graphene derivatives incorporating pyridinic nitrogen. The synthesis and electronic properties of nitrogen-doped graphene (N content: 9.8%), featuring both localized spin centers and spin-containing sites with itinerant electron properties, are reported. This material exhibits spin-switch behavior (on–off–on) controlled by microwave irradiation at X-band frequency. This phenomenon may enable the creation of novel types of switches, filters, and spintronic devices using sp^2-only 2D systems.

Spintronics is a developing field of electronics that exploits both the charge and the spin of electrons to perform logic operations and to process, store, and transmit information.[1] Because spin-polarized currents encode more information than charge alone, a diverse spectrum of efficient spintronic logic, transmission, and storage devices have been envisaged, including spin-field-effect transistors, spin-light-emitting diodes, spin-resonant tunneling components, spin modulators and encoders, and quantum bits. They are expected to have many advantages over traditional semiconductor-based alternatives, including higher data processing speeds, lower power consumption, nonvolatility, and higher integration densities.[2] A central goal of spintronics is to identify materials exhibiting spin-dependent effects, which are required for the occurrence of spintronic processes.[1] Graphene was recently suggested to be an attractive platform for spintronic applications[3–5] because it exhibits several spin-related phenomena including tunnel magnetoresistance,[6] enhancement of spin-injection efficiency,[7] the Rashba effect,[8] the quantum spin Hall effect,[9] and large perpendicular magnetic anisotropy.[10] It also exhibits several properties useful in spintronics, including ballistic charge transport,[11] long spin lifetimes and spin-diffusion lengths,[12,13] limited hyperfine interactions,[14] gate-tunable magnetic order,[15] and weak spin–orbit coupling.[3] Due to its exceptionally long spin lifetime of ≈10 ns (corresponding to a spin-diffusion length of several micrometers at room temperature), graphene has an intriguing spin-conserving potential. It is thus regarded as a promising material for spin transport in spin-valve architectures, enabling faithful transmission of information encoded in a carrier's spin across a device.[4] However, because of its diamagnetism and weak spin–orbit coupling,[16] it exhibits only weak transport-current-induced spin densities and weakly spin-polarized currents. Pristine graphene cannot function as a spin generator or an injector of spin-polarized carriers,[4] but strain induced in the material arising from surface corrugation and lattice mismatch between graphene layers and underlying substrates can severely change the electronic, magnetic, and transport properties.[17,18] Strain effects are known to promote modification of the graphene bandgap and can induce spin gap asymmetry and spin-polarization effects, locally or even extended over the 2D carbon network;[17,19] thus the "strain engineering" approach bears great potential for its application in graphene-based nanofabrication technologies.[18,20] For example, Yan et al. have shown that cooperativity between strain and out-of-plane distortion in the graphene wrinkles provide valley-polarized sites with significant energy gaps, a property that offers the ground for realization of high-temperature "zero-field" quantum valley Hall effects.[21] Liu et al., upon interfacing graphene with orthorhombic black phosphorus (BP), demonstrated that both lattices can be mutually
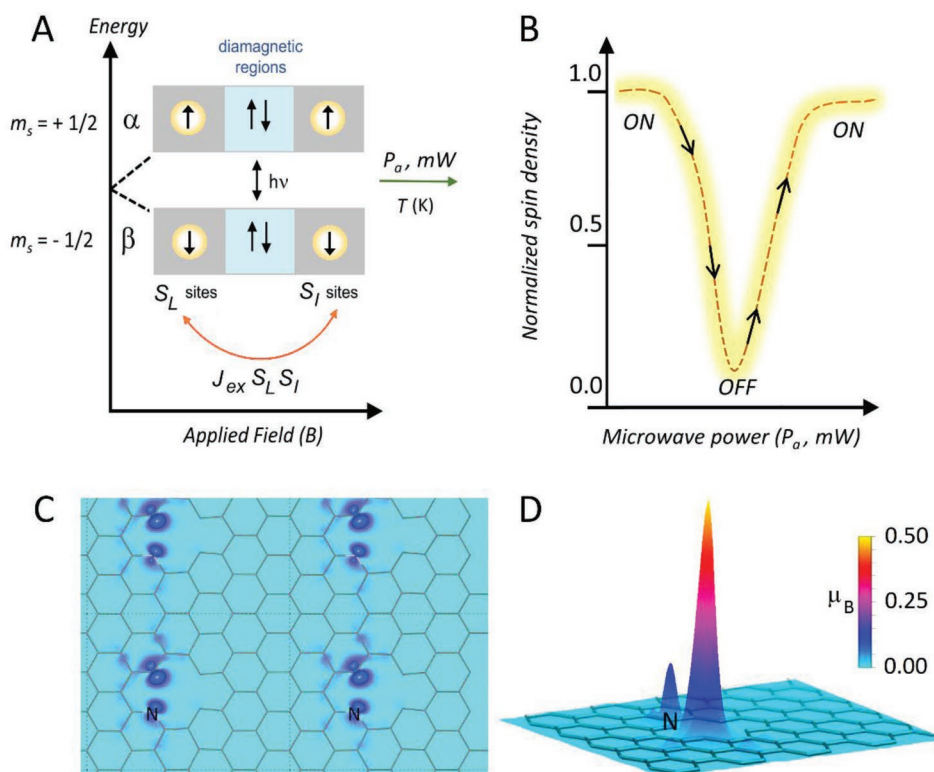
Dr. G. Zoppellaro, Dr. A. Bakandritsos, Dr. P. Błoński, Dr. P. Lazar,
T. Steklý, Dr. A. Opletalová, Prof. M. Otyepka, Prof. R. Zbořil
Department of Physical Chemistry
Regional Centre of Advanced Technologies and Materials
Faculty of Science
Palacký University Olomouc
Šlechtitelů 27, 78371 Olomouc, Czech Republic
E-mail: zoppellarogiorgio@gmail.com; radek.zboril@upol.cz
Dr. J. Tuček, Z. Baďura
Department of Experimental Physics
Regional Centre of Advanced Technologies and Materials
Faculty of Science
Palacký University Olomouc
Šlechtitelů 27, 78371 Olomouc, Czech Republic
Dr. T. Susi
Faculty of Physics
University of Vienna
Boltzmanngasse 5, 1090 Vienna, Austria

Figure 1. The spin-switch effect in pyridinic N-doped graphene is driven by the exchange interaction between two spin domains. A) Model of two distinct spin systems (the S_L and S_I sites) embedded in nitrogen-doped graphene, separated by a diamagnetic region, showing the effective spin polarization and transitions between the two electronic Zeeman levels ($\pm\frac{1}{2}$) in an external magnetic field (B) with an appropriate phonon energy ($h\upsilon$). When the exchange interaction (J_{ex}) exceeds k_BT and under the application of large microwave flux density (P_a), spin-flip-flop transitions from uncoupled and saturated S_I and S_L sites intercross the energy band of the coupled system (S_IS_L). B) This causes spin injection of polarized electrons into the S_IS_L band. C) First-principles DFT calculations show the theoretical charge density distribution in the spin-up channel corresponding to the energy range between −0.5 eV and Fermi energy (E_F) in the density of states (DOS) plot shown in Figure 2D and in Figures S2 and S3 (Supporting Information). The Vienna Ab-initio simulation package (VASP, a cutoff energy of 600 eV) and the Perdew–Burke–Ernzerhof (PBE) approximation were used. The extent of the computational cell is indicated by the dashed lines. D) Calculated magnetic moment (in μ_B) distribution within the cell, corroborating the charge density distribution shown in (C).

strained and sheared in such a way to create periodically fluctuating pseudomagnetic fields (PMFs), and valley polarization could be manipulated by application of an external magnetic field, offering a route for developing a valley filter (valleytronics).[22] However, to create graphene spintronic devices without the underneath aid of inorganic ferromagnetic substrates, one must embed diverse spin-polarized domains directly into the graphene backbone. Spin-valve behavior, which is fundamental to spintronics, requires the presence of two types of spin components (see **Figure 1**A): i) localized spin centers (S_L) and ii) spin-containing sites with itinerant electron properties (S_I). Furthermore, these spin systems must interact within the molecular framework (J_{ex}).

A major challenge is to identify or create systems in which these spin components coexist and are spatially separated while maintaining an intimate electronic interaction. Several strategies for altering the electronic/magnetic and spin-related properties of graphene have been evaluated. These include doping/substitution of the graphene lattice with non-carbon atoms, adsorption of atoms, sp^3 functionalization, edge engineering, and spatial confinement.[16] Functionalization is very effective at enhancing spin–orbit coupling, imprinting, and stabilizing

ferromagnetic or antiferromagnetic order at relatively high temperatures.[16,23–26] However, it introduces disorder and sp^3 defects that restrict charge mobility and reduce the spin relaxation length.[27,28] Theoretical studies indicate that while spatial confinement and edge engineering can induce the emergence of polarized spins and currents, this is most likely to occur in graphene nanoribbons below a threshold width, with a specific edge geometry[29–32] or edge functionalization (e.g., graphene nanoribbons functionalized with stable spin-bearing radical groups).[33] Therefore, despite its challenges,[34,35] doping with n- or p-type heteroatoms may be the most practical way to equip graphene with localized spins while maintaining a charge carrier concentration high enough to preserve its conductivity. In this context, nitrogen doping is envisioned as a method to imprint active centers into graphene to create materials suitable for organic-based spintronics.[36–40] Błoński et al.[36] recently reported that ferromagnetic spin ordering emerges in graphene doped with graphitic nitrogen. Conversely, Ito et al.[38] reported that pyrrolic nitrogen reduced the effective spin content of graphene and suppressed its magnetic response. However, the influence of pyridinic nitrogen on the evolution of magnetic features in graphene and its effects on potential spintronic

behavior are unstudied. More importantly, due to the electron-donating nature and spin-inducing capability of nitrogen in graphene, 2D systems doped with pyridinic N could contain both spin-generating and spin-conserving regions and could thus operate in the spin-injection and spin-transport regimes simultaneously, opening a route to advanced multifunctional spintronic materials.[4]

In this work, we report a new graphene-based material containing extensive pyridinic N-doping that acts as spin switch, in an "on–off–on" fashion, under microwave energy. Two spin systems with distinct natures (the S_L and S_I fractions) coexist within this material, as predicted by first-principles calculations (Figure 1C,D; Figures S1–S3, Supporting Information). We observed that spin flip-flop processes arising from relaxation of the magnetic moments of the S_L and S_I fractions intercrossed the energy band associated with the exchange-coupled (J_{ex}) high-spin system, $S_I S_L$. Polarized spin transfer occurred below a threshold temperature (T) when the material was exposed to a sufficiently high microwave flux density (P_a), which caused a dramatic increase in the net spin polarization of the high-spin component. Pyridinic ^{14}N-doped graphene (pNG) is thus a microwave energy-driven spin-switch material (Figure 1B), with intrinsic spin-dependent properties that arise from its chemical structure and can be manipulated at X-band frequency using microwaves. Electric and magnetic fields are commonly used to modulate spin injection in spin-valve systems; our results demonstrate for the first time that microwave irradiation can be used for this purpose in graphene-based spin-valve architectures.

To produce graphene with a high content of pyridinic motifs, a system with high content of vacancies would be required. Preliminary studies in our laboratory established the formation of vacancies upon chemical treatment of fluorographene (FG); therefore, we attempted to prepare highly pNG using the versatile chemistry of FG.[25,41–44] FG was reacted with hydroxylamine (NH_2OH) at 130 °C in dimethylformamide (DMF), avoiding high-temperature treatment or highly reactive reagents, used previously.[45–47] The Supporting Information presents a detailed characterization of pNG and the mechanism of its formation, which involves: i) the defluorination of FG and its transformation into highly N-doped (9.8 at.%) graphene (see Figure S4A–D in the Supporting Information); ii) the decomposition of hydroxylamine into ammonia, (identified by trapping the byproducts of the reaction, as described in Figure S4E in the Supporting Information), which undergoes dehydrogenation at vacancies[48–50] and is thus a source of the atomic nitrogen that becomes doped into the graphene lattice; iii) the in situ formation of lattice vacancies in FG (see Figure S5A,B in the Supporting Information); and iv) the formation of a predominantly sp² architecture (Figure S5C,D, Supporting Information). Atomic force microscopy (AFM) and transmission electron microscopy (TEM) indicated that pNG consisted mainly of nanosized flakes (**Figure 2**A; Figure S6, Supporting Information). Figure 2B,C shows carbon and nitrogen elemental mappings of pNG flakes obtained by scanning transmission electron microscopy/energy-dispersive X-ray spectroscopy (STEM–EDS), revealing that the material exhibits very homogeneous N-doping (within the limit of the instrument resolution of a few nanometers). This was attributed to

the well-defined stoichiometry of FG, which ensures that all carbon centers in the starting material are equally susceptible to transformation. As predicted by first-principles calculations (Figure 2D; Figures S1–S3, Supporting Information), pyridinic nitrogen motifs enable the emergence of two interacting spin populations: i) a strong spin-up channel near the Fermi energy (E_F), corresponding to ferromagnetically interacting localized spins (S_L) consisting predominantly of the in-plane p_{xy} orbitals of the undercoordinated carbons in divacancies (DV), and ii) the valence band, which is dominated by delocalized Cp_z electrons (the S_I spin population) and overlaps with the S_L population, as shown in Figure 2D. In addition, small magnetic moments are present on carbon atoms near DV defects and between defects (Figure 1C,D), where the charge/spin densities are more dispersed (delocalized) along the σ-bonds. The system has a very small electron gap, which is on the order of several tens of meV and could be further reduced or even closed in the presence of graphitic nitrogen (as discussed in the following). Consequently, a relatively mild stimulus should be enough to induce the injection of spin-up electrons into the conduction band.

The predominantly pyridinic character of the nitrogen dopants in pNG was verified experimentally using three independent techniques. First, scanning tunneling medium-angle annular dark-field (STEM-MAADF) and electron energy loss spectroscopy (EELS) analyses indicated that the background-subtracted N K response of pNG is consistent with pyridinic N (Figure 2E).[51] Second, the pH dependence of the apparent surface charge (ζ_p, zeta potential) of a pNG suspension in water indicated that the material's point of zero charge is ≈5.3 (Figure 2F), coinciding with the pK_a of pyridine (5.2).[52] Third, the N1s high-resolution X-ray photoelectron spectroscopy (HR-XPS) spectrum of the partially protonated (as-prepared) pNG features two N components (Figure 2F, left spectrum): a low binding energy (BE) component attributed to pyridinic N and a high BE component that could be attributed to either pyrrolic N or protonated pyridinic N; N-protonation is known to increase BE.[53] Conversely, the N1s spectrum of pNG deprotonated by repeated alkaline washings (Figure 2F, right spectrum) could be fitted with a single symmetric Gaussian component with a BE typical for pyridinic N. In this case, a minor high BE (402 eV) component attributed to graphitic N was observed, which was reported to reduce further the bandgap.[36] Finally, theoretical modeling of the IR spectra corroborated the assignment of the pyridinic configuration (Figure S7, Supporting Information).

The predicted difference in the nature of the S_L and S_I spin-containing domains was verified experimentally by electron paramagnetic resonance spectroscopy (EPR) experiments using pNG samples doped with ^{14}N (p-^{14}NG) and samples isotopically enriched with ^{15}N (p-^{15}NG). EPR results unveiled the importance of the presence of nitrogen nuclear hyperfine fields (I_N) for the emergence of the "on–off–on" spin-switch behavior. Specifically, the EPR spectrum of p-^{14}NG ($T = 118$ K, 0.3 mW, **Figure 3**A-i) is consistent with an organic-based radical, featuring a sharp Lorentzian-type derivative signal ($\Delta B_{pp} = 13.0$ G; Figure S10A, Supporting Information) centered at a g_{eff} of 1.997. This signal is complemented by broad wings that develop asymmetrically in the low and high field regions. The overall signal could not be simulated using perturbation theory in the spin-Hamiltonian framework by a single $S = 1/2$
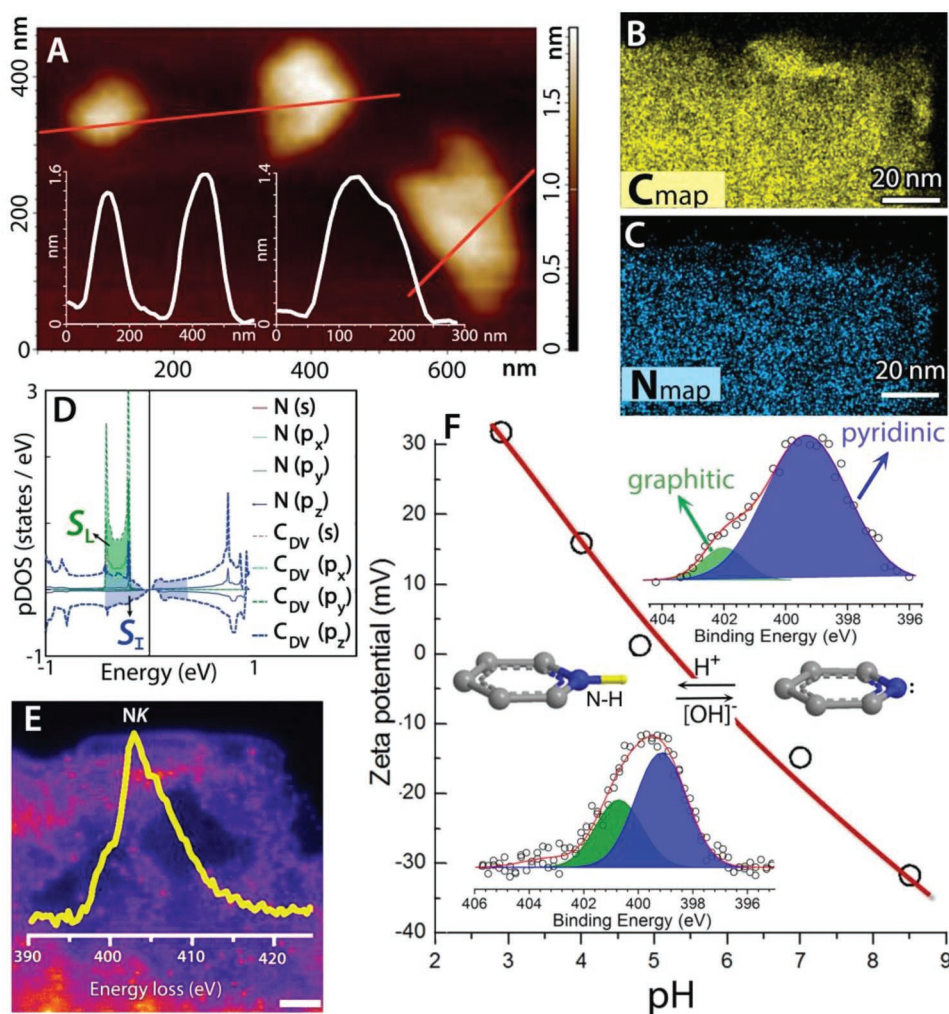
Figure 2. Characterization of pyridinic N-doped graphene (pNG). A) AFM image of pNG on mica support, showing single layer graphene nanoflakes. The insets show the flakes' height profiles. B,C) STEM–EDS elemental mapping of a pNG nanoflake for carbon (B) and nitrogen (C). D) Orbital-resolved partial theoretical DOS of graphene doped with pyridinic N. C_{DV} denotes carbon atoms adjacent to a DV defect, and energies are quoted relative to E_F. E) STEM-MAADF image of a region near the edge of a pNG nanoflake and (overlay) the corresponding background-subtracted nitrogen electron energy loss spectrum. Scale bar: 1 nm (see also Figure S8 in the Supporting Information). F) Apparent surface charge (zeta potential) of an aqueous pNG suspension as a function of pH. Insets show the deconvoluted N1s HR-XPS spectra of the protonated (left) and deprotonated (right) pNG.

transition, whether of Gaussian, Lorentzian, or Voigt-shape type. Instead, the resonance appears to be a superposition of: i) a narrow Lorentzian-component (Figure 3A-i; simulated in Figure S10A (Supporting Information)_with an isotropic g-tensor of 1.997) and ii) a broad Gaussian component with an anisotropic g-tensor (g_1 of 2.060, $g_{2,3}$ of 1.997, and g_{eff} = 2.018; red line in Figure 3A-i). The Lorentzian component is related to localized unpaired electrons (S_L) that experience strong exchange regime, resulting in a narrow signal, negligible zero field splitting, and no appreciable interaction with the ^{14}N atoms (and thus do not give rise to any hyperfine term in the Hamiltonian expression, $\hat{H} = \beta_e g\hat{S}B_0 - \Sigma_n 2J\hat{S}_L\hat{S}_{L-1}$. The broad signal is associated with p-^{14}NG to itinerant $S = 1/2$ electrons. Here, the hyperfine terms with nearby ^{14}N nuclei are active but remain poorly resolved and are thus responsible for the observed resonance field broadening ($\hat{H} = \beta_e g\hat{S}_I B_0 - \Sigma_n 2J\hat{S}_I\hat{S}_{I-1} + \Sigma_n \hat{S}_I A_N I_N$). Because of these nuclear hyperfine interactions, the

spin–spin relaxation time calculated for the Gaussian component was appreciably shorter ($T_2 \approx 0.4 \times 10^{-9}$ s) than that for the noninteracting Lorentzian component ($T_2 \approx 0.5 \times 10^{-8}$ s). To confirm the presence of the N-hyperfine field interactions, we recorded the EPR spectrum of p-^{15}NG, whose hyperfine interactions differ from those of p-^{14}NG because the nuclear spin of ^{15}N is $I = 1/2$ whereas that of ^{14}N is $I = 1$. Two distinct spin components were also observed in the p-^{15}NG spectrum: one Lorentzian (simulated in Figure S10B in the Supporting Information) and one Gaussian (red line in Figure 3B-i). However, a simulation of the broad component in the spin-Hamiltonian framework using second-order perturbation theory (Figure 3B, red trace, g_1 of 2.009, $g_{2,3}$ of 1.997, and g_{eff} = 2.001) predicted it to have weaker signal asymmetry and a smaller resonance-field spread (ΔB of 500 G for p-^{15}NG vs ΔB of 700 G for p-^{14}NG) than the corresponding component in the p-^{14}NG spectrum. These results are in harmony with the weaker hyperfine field

**ADVANCED
SCIENCE NEWS**

www.advancedsciencenews.com
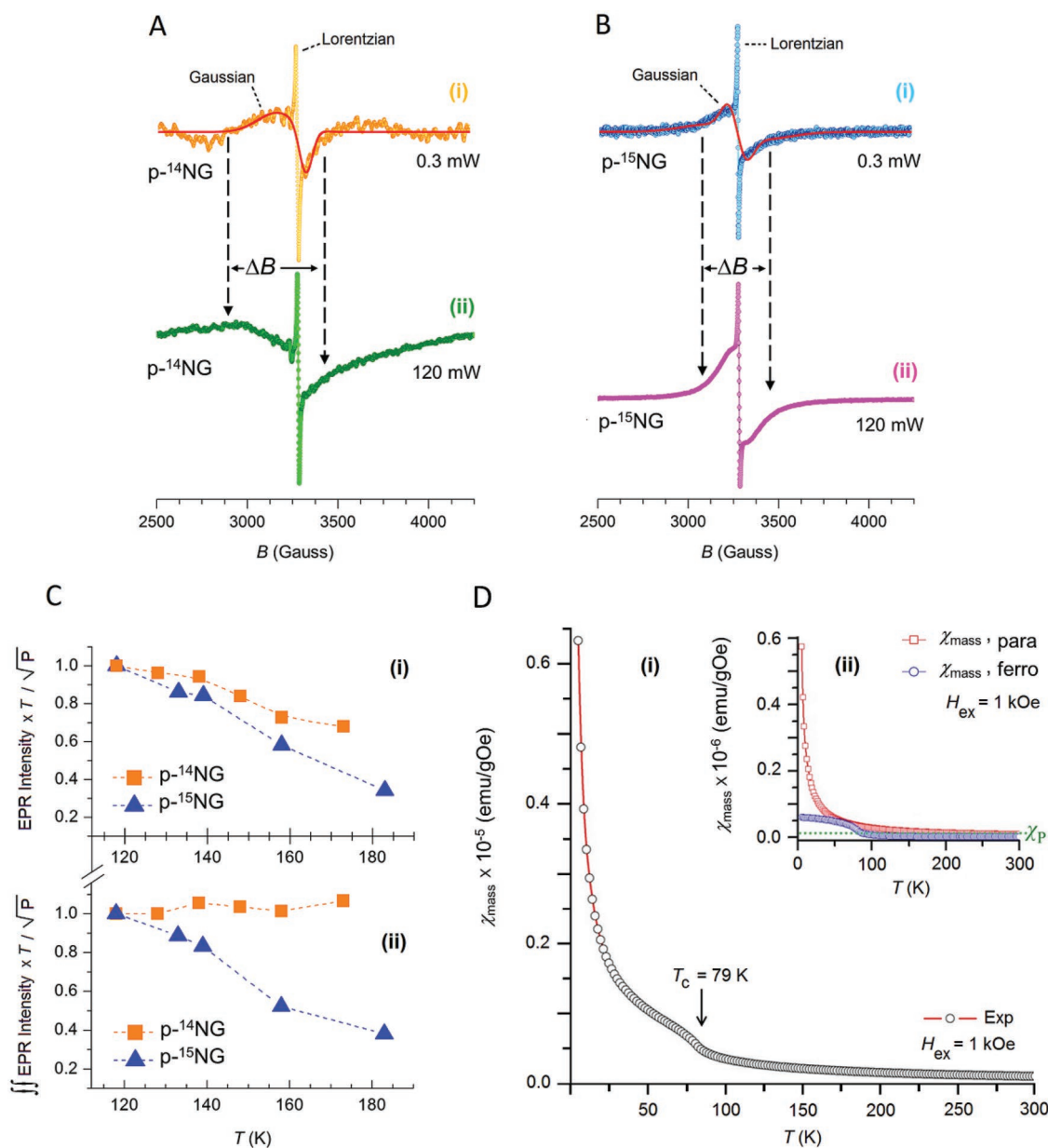
**ADVANCED
MATERIALS**

www.advmat.de

Figure 3. The two types of spin domains in pNG materials and their magnetic behavior revealed by EPR and bulk susceptibility. X-band (9.1–9.2 GHz, 100 kHz modulation frequency) EPR spectra of the N-doped graphene materials recorded at $T = 118$ K. A) p-^{14}NG recorded at: i) 0.3 mW and ii) 120 mW. B) p-^{15}NG recorded at: i) 0.3 mW and ii) 120 mW. All samples were analyzed in a freshly dispersed frozen matrix of DMF. The red lines show the results of simulations of the broad component (S_I) using the parameters specified in the text. C) Temperature dependence of the spin concentration in p-^{14}NG (square) and p-^{15}NG (triangle) for: i) the Lorentzian component alone (intensity-based: $I_{EPR} \times T/\sqrt{P}$ vs T) and ii) the Gaussian (S_I) and Lorentzian (S_L) components combined (total area-based, $\iint I_{EPR} \times T/\sqrt{P}$ vs T). D-i) Mass magnetic susceptibility, χ_{mass}, versus T of p-^{14}NG, measured under an external magnetic field of 1 kOe; D-ii) mass magnetic susceptibility for paramagnetic, $\chi_{mass,para}$, and ferromagnetic, $\chi_{mass,ferro}$, fraction as a function of temperature.

associated with ^{15}N nuclei ($I = 1/2$). The presence of stronger hyperfine interactions in the p-^{14}NG system for the generation and control of an "on–off–on" spin-switch behavior became apparent upon recording the EPR signals of p-^{14}NG (Figure 3A-ii) and p-^{15}NG (Figure 3B-ii) at higher microwave power levels ($P_a = 120$ mW). The entire resonance spectrum of p-^{15}NG exhibited only a slight symmetric broadening at high P_a, without indication of significant shift in g_{eff}; this indicates a small energy spread (ΔE) associated with the ground $\langle\downarrow\rangle$

and excited $\langle\uparrow\rangle$ energy levels of the two spin configurations in both domains, S_I and S_L. In contrast to an isolated atom where unpaired electrons can interact only with one nucleus, the electrons confined in pNG can interact with several N lattice nuclei with different strength (through Fermi contact and dipolar couplings), similarly as being immersed in a bath of nuclear spins.[54] The hyperfine spin-Hamiltonian ($\hat{H} = \Sigma_n \check{S}_I A_N I_N$) for S_I can be viewed, in the simplest scenario with uniform hyperfine couplings, as a Heisenberg-type spin function. The isotropic

**ADVANCED
SCIENCE NEWS**

www.advancedsciencenews.com

**ADVANCED
MATERIALS**

www.advmat.de

hyperfine interaction for electrons in an s-type conduction band in which the Fermi contact part dominates has been described as $\hat{H} = \Sigma_n \check{S}_I A_N I_N = \check{S} \times \boldsymbol{h}$, with $\boldsymbol{h} = \Sigma_n A_N I_N$ and $A = 4/3 \, (\mu_0 g_I \mu N \mu_B |u_0|^2)$ with u_0 being the Bloch function amplitude. For s-type conduction band electrons, the effective magnetic field $\boldsymbol{h}$ induced by nuclei onto the electron spin moment is referred to as the Overhauser field.[55] Small distribution in $\boldsymbol{h}$ produces narrow Overhauser fields and decreases the so-called electron spin decoherence effect induced by hyperfine terms, which is the decay of phase information encoded in the electron spin.[56] We hypothesize that in p-^{15}NG there exists only a small quantum admixture of the S_I and S_L wavefunctions; the distribution in Overhauser field ($\boldsymbol{h}$) is small for S_I; and the S_I and S_L magnetic relaxation regimes are weakly perturbed by their mutual presence in the lattice, as can be seen later in the power-saturation experiments. On the contrary, for p-^{14}NG, the entire resonance signal exhibits an extreme broadening at high P_a and at 118 K (i.e., a very pronounced increase in the magnetic field spread, ΔB, which reached $\approx$1750 G) being accompanied by clear shift in g-value ($g_{eff} \approx 2.030$). This phenomenon suggests a larger energy spread of the pertinent S_I states (large $\boldsymbol{h}$ spread) owing to the large perturbation of the electron-spin moments by stronger anisotropic fields from the ^{14}N-nuclear hyperfine components ($I = 1$). Additional EPR spectra are given in the Supporting Information (EPR traces for p-^{14}NG in Figures S11–S14 and for p-^{15}NG in Figures S15–S17 in the Supporting Information).

Analysis of the variation of the spin concentration in p-^{14}NG and p-^{15}NG versus temperature (see Figure 3C and Figures S18 and S19 in the Supporting Information) gives further insight of the temperature-dependent behavior associated with the S_I and S_L spin domains. For the Lorentzian component (S_L), the temperature dependence of the EPR intensity-based spin concentration departed from Curie behavior in both systems, p-^{14}NG (experimental data: squares, Figure 3C-i) and p-^{15}NG (experimental data: triangles, Figure 3C-i), which is indicative of the strong exchange regime ($J_{ex1} S_L \cdot S_L$) with ferromagnetic interactions ($I_{EPR} \times T/\sqrt{P} \neq C$, with C being the Curie constant). However, the temperature dependence of the total EPR signal area–based spin concentration (which is dominated by the broad S_I component rather than the narrow S_L one) revealed clear differences between p-^{14}NG and for p-^{15}NG (Figure 3C-ii). The p-^{15}NG system keeps the ferromagnetic behavior (Figure 3C-ii, triangles), and both S_L and S_I domains exhibit ferromagnetic character. Here the exchange interaction (J_{ex1}) for the $S_L \cdot S_L$ domains and (J_{ex2}) for the $S_I \cdot S_I$ domains dominate over the cross-exchange term ($J_{ex1,2}$) $S_I \cdot S_L$, in agreement with the proposed small quantum admixture of the S_I and S_L spin-wavefunctions. The p-^{14}NG system, on the contrary, followed a Curie trend (Figure 3C-ii, squares). The latter result suggests that in p-^{14}NG the S_I systems are perturbed more substantially by large anisotropic hyperfine fields; hence, the cross-exchange term ($J_{ex1,2}$) associated with the $S_I \cdot S_L$ spin configuration dominates; in particular, besides the ferromagnetic (S_L) domain seen in the sharp Lorentzian component, the S_I domain shows a dominant Pauli-type (temperature-independent) behavior. This effect must originate from a more efficient quantum admixture of the S_I domains with part of the S_L sites in p-^{14}NG, forming $S_I \cdot S_L$, a Fermi-degenerate 2D electron system. Electronic

fingerprints of this type are typical of conducting electrons with Pauli character (Fermi-degenerate electron systems).[57] The presence of such electrons is consistent with our theoretical calculations, which correlated the S_I spin population with the valence band derived primarily from the delocalized Cp_z (and Np_z) electrons (Figure 2D). The coexistence of distinct spin systems in p-^{14}NG was also confirmed by recording the temperature dependence of the mass magnetic susceptibility (χ_{mass}) (Figure 3D) and its hysteresis loop at 5 K (Figure S20, Supporting Information). In accordance with the EPR data, two magnetically diverse regions were identified, with overlapped contribution; one characterized by significant magnetic interactions that promote ferromagnetic ordering at low temperature ($\approx$79 K), and a second domain, exhibiting temperature-independent contribution (in the degenerate limit) from conduction (itinerant) electrons. The latter behavior was fully consistent with the conduction-electron fraction responsible for the Gaussian component observed in the EPR spectra. To investigate further the different magnetic behavior of p-^{14}NG and p-^{15}NG at high microwave power, we studied the total area-based spin concentrations (**Figure 4**A) upon increasing the applied microwave energy flux, P_a (i.e., their saturation behavior).

For p-^{15}NG, the net spin concentration decreased substantially as P_a increased which was well described by Portis and Castner's theory[58,59] (Equation (S1) in the Supporting Information). Fitting based on this theory (see the solid lines in Figure 4A) indicated that the spin packets associated with the S_I and S_L components are not cross-correlated, i.e., the sharp and broad components of Figure 3B behave as independent (noncorrelated) spin domains. The fitting analysis yielded the following estimated values at 143 K ($P_{1/2} = 158.7$ mW, $b = 1.6$), at 133 K ($P_{1/2} = 84.6$ mW, $b = 1.6$), and at 118 K ($P_{1/2} = 63.2$ mW, $b = 1.6$). As expected, the half-saturation value ($P_{1/2}$) decreases upon lowering the temperature, in full agreement with the theory. The value obtained for the shape factor b is also consistent with the analysis of the EPR resonance envelopes, characterized by an admixture of Gaussian and Lorentzian lines, and further validates the conclusion that the S_I and S_L spin components are magnetically uncorrelated (i.e., when spin systems exhibit $b > 1$).[60,61] The recorded evolution of the power saturation EPR traces in p-^{15}NG, obtained at 118, 133, and at 143 K, are given in the Supporting Information (Figures S21–S23, Supporting Information). The power saturation behavior of p-^{14}NG was, indeed, very different from that expressed by p-^{15}NG (Figure 4A). At high temperature (at 143 and at 133 K), the EPR resonance lines saturate much faster than those observed for p-^{15}NG, giving, from fitting analysis, the following values of $P_{1/2} = 15.5$ mW, $b = 1.0$ at 143 K, and $P_{1/2} = 13.2$ mW, $b = 1.33$ at 133 K. At 123 K, the saturation behavior of p-^{14}NG could not be analyzed in the framework of the Portis and Castner's theory. At this temperature, the spin population in p-^{14}NG decreased sharply until the applied microwave power reached 11 mW, at which point it increased sharply before plateauing when the microwave power reached 91 mW. This behavior is unprecedented and suggests the occurrence of an "on–off–on" transfer of polarized spins, thus interpreted in terms of spin-switch effects (see Figures S24–S26 in the Supporting Information for the power saturation EPR traces of p-^{14}NG at
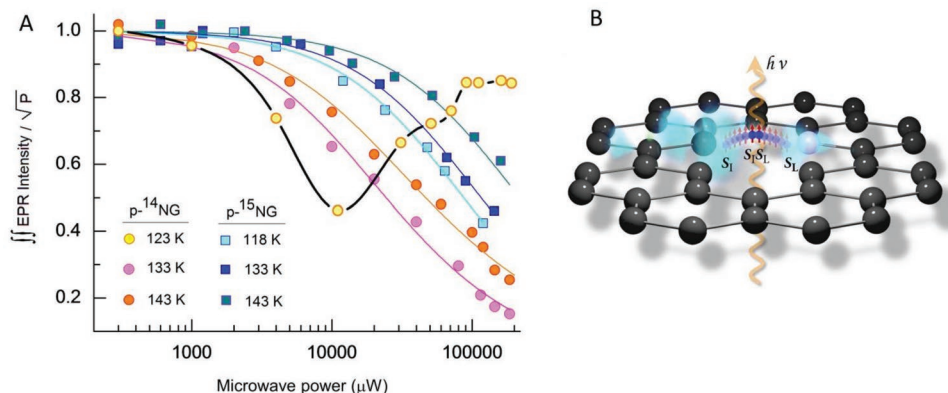
**ADVANCED
SCIENCE NEWS**

www.advancedsciencenews.com

**ADVANCED
MATERIALS**

www.advmat.de

Figure 4. The microwave-induced spin-switch effect in pNG. A) EPR power saturation plot showing the emergence of the spin-switch phenomenon in p-^{14}NG (experimental data, circles) at low temperature (123 K) compared to its normal saturation behavior expressed at higher temperatures (133 and 143 K). The saturation trend of p-^{15}NG (experimental data, squares), on the contrary, follows at all probed temperatures (118, 133, and 143 K) the saturation behavior expected from the theory. The plots are based on analysis of the EPR spectra considering the entire resonance line ($\iint I_{EPR}/\sqrt{P}$), normalized against the maximum observed intensity. The solid lines in the data plots result from fitting analysis of the data according to the Portis and Castner's theory. The black line for p-^{14}NG at 123 K is given here as guide to the eye. B) Schematic representation of the population of the $S_L S_I$ band with spin-polarized electrons upon increasing the applied microwave power.

123, 133, and 143 K). The phenomenon was explained by proposing that the new exchange-coupled high-spin state ($S_I S_L$) is populated (beyond its normal Boltzmann distribution) when T is sufficiently low and J_{ex} exceeds the available thermal energy ($k_B T \leq 123$ K). These interactions are reminiscent of those seen in metals and semiconductors, where the conduction electrons (the S_I in this case) are bound to localized spins (the S_L in this case) via an exchange energy interaction (J_{ex}).[62,63] In p-^{14}NG, flip-flop transitions may connect the power-saturated S_I and S_L states with the new unsaturated $S_I S_L$ coupled state, transferring local field energy away from the saturated states and resulting in polarized spin injection when P_a exceeds a certain threshold. This dynamic process of feeding $S_I S_L$ then plateaus at ≈91 mW (Figure 4A), at which point P_a and dP_a/dB become proportional to H_1^2 (Equation (S7), Supporting Information) and the thermodynamic process of relaxation occurs again in accordance with the Portis and Castner's saturation theory. Because this phenomenon is not observed in p-^{15}NG, the exchange interaction ($J_{ex1,2}S_I S_L$) must be mediated by the anisotropic $AI_N S$ terms (originating from the interactions with the strong p-^{14}N nuclear hyperfine fields), which are key for the through-bond propagation of spin-polarization and quantum admixture of the S_I and S_L states.

These experimental results were in full agreement with the theory-based prediction that graphene doped with pyridinic N would contain two spin populations on p_{xy} and p_z orbitals that overlap in energy, with the latter extending very close to and above the Fermi level (the S_L and S_I populations, respectively). The experimental observation of multiple strong p-^{14}NG nuclear hyperfine interactions with the p_z spins should be considered responsible for the wide energy distribution of the p_z density of states (DOS) in the density functional theory (DFT) calculations. These features, along with the very small bandgap in DOS, enable the $S_L \cdot S_I$ interaction and the injection of spin-polarized electrons (given a sufficient microwave flux density) to an energy level lying extremely close to the conduction band (the coupled $S_I \cdot S_L$ state), generating a microwave-controlled

spin switch, as illustrated in Figure 4B. From the analysis of the (three) as–synthesized batches of the p-^{14}NG material, we observed that while the spin-switch behavior was clearly expressed at the same temperature threshold (123 K) in all cases, the power-dependent switching effect became active (in one batch) under microwave irradiation flux, P_a, as low as 4 mW at $T = 123$ K, (see Figures S27 and S28 in the Supporting Information). This observation indicates that the hyperfine-dependent switching phenomenon is dictated by the subtle combination of the mutual distance (R) and angles (θ) between the spin domains S_I and S_L belonging to the different sublattices, $J_{ex1,2(SI \cdot SL)} \propto 1/R^3$ and $J_{ex1,2(SI \cdot SL)}(R) \propto \sin^2(\theta)_{SI \cdot SL}$,[64] as well as by the effective number (N) of interacting S_I and S_L sites involved in the cross-exchange process (ΔN population of the coupled state modulate the spin-lattice relaxation term, T_1, and in turn dictates changes in P_a; see Equations (S2), (S6) and (S7) in the Supporting Information). This is clearly one of the limits of the "wet-chemistry" synthetic methodology, because the exact positioning in the lattice of the doping nitrogens (and spin containing S_L sites) cannot be achieved with atomic precision.

The results presented in this work pave the way to sp^2-only 2D systems exhibiting spin-switch behavior induced at X-band frequencies by microwave energy. The possible doping of graphene with other elements e.g., phosphorous[65,66] (^{31}P, $I = \frac{1}{2}$, natural abundance 100%, a nuclear magnetic moment $\mu_I/\mu N$ of 1.1316) or arsenic (^{75}As, $I = 3/2$, natural abundance 100%, nuclear magnetic moment $\mu_I/\mu N$ of 1.4395),[67] which encode nuclear hyperfine fields of different strengths, may offer further possibilities for investigating the impact of hyperfine interactions and application of microwave energy on the emergence of spin-switch behavior in organic materials. Controlled spin-switch behavior (On–Off) and transport properties are the current focus of research in several laboratories (in academy and industry) for devising a new generation of graphene-based transistors. These materials and devices have shown some promise, as well as several limitations, for future development in semiconductor electronics, for digital logic and radio-frequency (RF) devices.[68,69] Carbon nanotubes

in fact have been explored as potential building blocks for signal routing in future microwave networks,[70] and in high-frequency signal processing applications,[71] while graphene layers have been shown to be more suitable for building RF devices with high cutoff frequencies (acting as frequency filters).[72,73] Therefore, the results presented here may stimulate further research into the alternative generation and control of spin-polarized electron injection in graphene-based materials, enabling the potential assembly of a novel class of spintronic and field-effect transistor (FET) devices.

Supporting Information

Supporting Information is available from the Wiley Online Library or from the author.

Acknowledgements

Conflict of Interest

The authors declare no conflict of interest.

Keywords

[1] I. Žutić, J. Fabian, S. Das Sarma, *Rev. Mod. Phys.* **2004**, *76*, 323.
[2] S. A. Wolf, D. D. Awschalom, R. A. Buhrman, J. M. Daughton, S. von Molnár, M. L. Roukes, A. Y. Chtchelkanova, D. M. Treger, *Science* **2001**, *294*, 1488.
[3] W. Han, R. K. Kawakami, M. Gmitra, J. Fabian, *Nat. Nanotechnol.* **2014**, *9*, 794.
[4] D. Pesin, A. H. MacDonald, *Nat. Mater.* **2012**, *11*, 409.
[5] S. Roche, J. Åkerman, B. Beschoten, J.-C. Charlier, M. Chshiev, S. P. Dash, B. Dlubak, J. Fabian, A. Fert, M. Guimarães, F. Guinea, I. Grigorieva, C. Schönenberger, P. Seneor, C. Stampfer, S. O. Valenzuela, X. Waintal, B. van Wees, *2D Mater.* **2015**, *2*, 030202.
[6] E. Cobas, A. L. Friedman, O. M. J. van't Erve, J. T. Robinson, B. T. Jonker, *Nano Lett.* **2012**, *12*, 3000.
[7] W. Han, K. Pi, K. M. McCreary, Y. Li, J. J. I. Wong, A. G. Swartz, R. Kawakami, *Phys. Rev. Lett.* **2010**, *105*, 167202.
[8] Y. S. Dedkov, M. Fonin, U. Rüdiger, C. Laubschat, *Phys. Rev. Lett.* **2008**, *100*, 107602.
[9] C. L. Kane, E. L. Mele, *Phys. Rev. Lett.* **2005**, *95*, 226801.
[10] H. Yang, A. Duc Vu, A. Hallal, N. Rougemaille, J. Coraux, G. Chen, A. K. Schmid, M. Chshiev, *Nano Lett.* **2016**, *16*, 145.
[11] A. S. Mayorov, R. V. Gorbachev, S. V. Morozov, L. Britnell, R. Jalil, L. A. Ponomarenko, P. Blake, K. S. Novoselov, K. Watanabe, T. Taniguchi, A. K. Geim, *Nano Lett.* **2011**, *11*, 2396.
[12] T.-Y. Yang, J. Balakrishnan, F. Volmer, A. Avsar, M. Jaiswal, J. Samm, S. R. Ali, A. Pachoud, M. Zeng, M. Popinciuc, G. Güntherodt, B. Beschoten, B. Özyilmaz, *Phys. Rev. Lett.* **2011**, *107*, 047206.
[13] B. Dlubak, M.-B. Martin, C. Deranlot, B. Servet, S. Xavier, R. Mattana, M. Sprinkle, C. Berger, W. A. De Heer, F. Petroff, A. Anane, P. Seneor, A. Fert, *Nat. Phys.* **2012**, *8*, 557.
[14] C. Cervetti, A. Rettori, M. G. Pini, A. Cornia, A. Repollés, F. Luis, M. Dressel, S. Rauschenbach, K. Kern, M. Burghard, L. Bogani, *Nat. Mater.* **2016**, *15*, 164.
[15] D. A. Abanin, P. A. Lee, L. S. Levitov, *Phys. Rev. Lett.* **2006**, *96*, 176803.
[16] J. Tuček, P. Błoński, J. Ugolotti, A. K. Swain, T. Enoki, R. Zbořil, *Chem. Soc. Rev.* **2018**, *47*, 3899.
[17] S. Nigar, Z. Zhou, H. Wang, M. Imtiaz, *RSC Adv.* **2017**, *7*, 51546.
[18] N.-C. Yeh, C.-C. Hsu, M. L. Teague, J.-Q. Wang, D. A. Boyd, C.-C. Chen, *Acta Mech. Sin.* **2016**, *32*, 497.
[19] F. Guinea, M. I. Katsnelson, A. K. Geim, *Nat. Phys.* **2010**, *6*, 30.
[20] C. Si, Z. Sun, F. Liu, *Nanoscale* **2016**, *8*, 3207.
[21] W. Yan, W.-Y. He, Z.-D. Chu, M. Liu, L. Meng, R.-F. Dou, Y. Zhang, Z. Liu, J.-C. Nie, L. He, *Nat. Commun.* **2013**, *4*, 2159.
[22] Y. Liu, J. N. B. Rodrigues, Y. Z. Luo, L. Li, A. Carvalho, M. Yang, E. Laksono, J. Lu, Y. Bao, H. Xu, S. J. R. Tan, Z. Qiu, C. H. Sow, Y. P. Feng, A. H. C. Neto, S. Adam, J. Lu, K. P. Loh, *Nat. Nanotechnol.* **2018**, *13*, 828.
[23] R. R. Nair, M. Sepioni, I.-L. Tsai, O. Lehtinen, J. Keinonen, A. V. Krasheninnikov, T. Thomson, A. K. Geim, I. V. Grigorieva, *Nat. Phys.* **2012**, *8*, 199.
[24] J. Tuček, P. Błoński, Z. Sofer, P. Šimek, M. Petr, M. Pumera, M. Otyepka, R. Zbořil, *Adv. Mater.* **2016**, *28*, 5045.
[25] J. Tuček, K. Holá, A. B. Bourlinos, P. Błoński, A. Bakandritsos, J. Ugolotti, M. Dubecký, F. Karlický, V. Ranc, K. Čépe, M. Otyepka, R. Zbořil, *Nat. Commun.* **2017**, *8*, 14525.
[26] A. Avsar, J. Y. Tan, T. Taychatanapat, J. Balakrishnan, G. K. W. Koon, Y. Yeo, J. Lahiri, A. Carvalho, A. S. Rodin, E. C. T. O'Farrell, G. Eda, A. H. Castro Neto, B. Özyilmaz, *Nat. Commun.* **2014**, *5*, 4875.
[27] M. Wojtaszek, I. J. Vera-Marun, T. Maassen, B. J. van Wees, *Phys. Rev. B* **2013**, *87*, 081402(R).
[28] J. Balakrishnan, G. Kok Wai Koon, M. Jaiswal, A. H. Castro Neto, B. Özyilmaz, *Nat. Phys.* **2013**, *9*, 284.
[29] Y.-W. Son, M. L. Cohen, S. G. Louie, *Nature* **2006**, *444*, 347.

**ADVANCED
SCIENCE NEWS**

www.advancedsciencenews.com

**ADVANCED
MATERIALS**

www.advmat.de

[30] O. Hod, V. Barone, J. E. Peralta, G. E. Scuseria, *Nano Lett.* **2007**, *7*, 2295.

[31] E.-j. Kan, Z. Li, J. Yang, J. G. Hou, *J. Am. Chem. Soc.* **2008**, *130*, 4224.

[32] Y. Li, Z. Zhou, P. Shen, Z. Chen, *ACS Nano* **2009**, *3*, 1952.

[33] M. Slota, A. Keerthi, W. K. Myers, E. Tretyakov, M. Baumgarten, A. Ardavan, H. Sadeghi, C. J. Lambert, A. Narita, K. Müllen, L. Bogani, *Nature* **2018**, *557*, 691.

[34] C. N. R. Rao, K. Gopalakrishnan, A. Govindaraj, *Nano Today* **2014**, *9*, 324.

[35] U. N. Maiti, J. Lim, K. E. Lee, W. J. Lee, S. O. Kim, *Adv. Mater.* **2014**, *26*, 615.

[36] P. Błoński, J. Tuček, Z. Sofer, V. Mazánek, M. Petr, M. Pumera, M. Otyepka, R. Zbořil, *J. Am. Chem. Soc.* **2017**, *139*, 3171.

[37] Q. Miao, L. Wang, Z. Liu, B. Wei, F. Xu, W. Fei, *Sci. Rep.* **2016**, *6*, 21832.

[38] Y. Ito, C. Christodoulou, M. V. Nardi, N. Koch, M. Kläui, H. Sachdev, K. Müllen, *J. Am. Chem. Soc.* **2015**, *137*, 7678.

[39] A. P. Alegaonkar, A. Kumar, S. H. Patil, K. R. Patil, S. K. Pardeshi, P. S. Alegaonkar, *J. Phys. Chem. C* **2013**, *117*, 27105.

[40] A. L. Friedman, C. D. Cress, S. W. Schmucker, J. T. Robinson, O. M. J. van't Erve, *Phys. Rev. B* **2016**, *93*, 161409(R).

[41] A. Bakandritsos, M. Pykal, P. Błoński, P. Jakubec, D. D. Chronopoulos, K. Poláková, V. Georgakilas, K. Čépe, O. Tomanec, V. Ranc, A. B. Bourlinos, R. Zbořil, M. Otyepka, *ACS Nano* **2017**, *11*, 2982.

[42] D. D. Chronopoulos, A. Bakandritsos, P. Lazar, M. Pykal, K. Čépe, R. Zbořil, M. Otyepka, *Chem. Mater.* **2017**, *29*, 926.

[43] P. Lazar, C. K. Chua, K. Holá, R. Zbořil, M. Otyepka, M. Pumera, *Small* **2015**, *11*, 3790.

[44] R. Zbořil, F. Karlický, A. B. Bourlinos, T. A. Steriotis, A. K. Stubos, V. Georgakilas, K. Šafářová, D. Jančík, C. Trapalis, M. Otyepka, *Small* **2010**, *6*, 2885.

[45] D. Guo, R. Shibuya, C. Akiba, S. Saji, T. Kondo, J. Nakamura, *Science* **2016**, *351*, 361.

[46] J. Song, Z. Yu, M. L. Gordin, D. Wang, *Nano Lett.* **2016**, *16*, 864.

[47] D. Deng, X. Pan, L. Yu, Y. Cui, Y. Jiang, J. Qi, W.-X. Li, Q. Fu, X. Ma, Q. Xue, G. Sun, X. Bao, *Chem. Mater.* **2011**, *23*, 1188.

[48] X.-F. Li, K.-Y. Lian, L. Liu, Y. Wu, Q. Qiu, J. Jiang, M. Deng, Y. Luo, *Sci. Rep.* **2016**, *6*, 23495.

[49] R. A. Bueno, J. I. Martínez, R. F. Luccas, N. R. del Árbol, C. Munuera, I. Palacio, F. J. Palomares, K. Lauwaet, S. Thakur, J. M. Baranowski, W. Strupinski, M. F. López, F. Mompean, M. García-Hernández, J. A. Martín-Gago, *Nat. Commun.* **2017**, *8*, 15306.

[50] B. Wang, L. Tsetseris, S. T. Pantelides, *J. Mater. Chem. A* **2013**, *1*, 14927.

[51] Y.-C. Lin, P.-Y. Teng, C.-H. Yeh, M. Koshino, P.-W. Chiu, K. Suenaga, *Nano Lett.* **2015**, *15*, 7408.

[52] H. Kiuchi, R. Shibuya, T. Kondo, J. Nakamura, H. Niwa, J. Miyawaki, M. Kawai, M. Oshima, Y. Harada, *Nanoscale Res. Lett.* **2016**, *11*, 127.

[53] D. Nolting, E. F. Aziz, N. Ottosson, M. Faubel, I. V. Hertel, B. Winter, *J. Am. Chem. Soc.* **2007**, *129*, 14068.

[54] M. Fuchs, V. Rychkov, B. Trauzettel, *Phys. Rev. B* **2012**, *86*, 085301.

[55] J. Schliemann, A. Khaetskii, D. Loss, *J. Phys.: Condens. Matter* **2003**, *15*, R1809.

[56] J. Jing, L.-A. Wu, *Sci. Rep.* **2018**, *8*, 1471.

[57] N. Fujita, D. Matsumoto, Y. Sakurai, K. Kawahara, H. Ago, T. Takenobu, K. Marumoto, *Sci. Rep.* **2016**, *6*, 34966.

[58] T. J. Castner Jr., *Phys. Rev.* **1959**, *115*, 1506.

[59] A. M. Portis, *Phys. Rev.* **1953**, *91*, 1071.

[60] G. Zoppellaro, A. Geies, K. K. Andersson, V. Enkelmann, M. Baumgarten, *Eur. J. Org. Chem.* **2008**, *8*, 1431.

[61] G. Zoppellaro, A. Geies, V. Enkelmann, M. Baumgarten, *Org. Lett.* **2004**, *6*, 4929.

[62] J. Winter, *Magnetic Resonance in Metals*, Clarendon Press, Oxford, UK **1971**.

[63] D. J. Lépine, *Phys. Rev. B* **1970**, *2*, 2429.

[64] M. Agarwal, E. G. Mishchenko, *Phys. Rev. B* **2019**, *99*, 085439.

[65] P. A. Denis, *Chem. Phys. Lett.* **2010**, *492*, 251.

[66] a) A. R. MacIntosh, G. Jiang, P. Zamani, Z. Song, A. Riese, K. J. Harris, X. Fu, Z. Chen, X. Sun, G. R. Goward, *J. Phys. Chem. C* **2018**, *122*, 6593; b) T. Susi, T. P. Hardcastle, H. Hofsäss, A. Mittelberger, T. J. Pennycook, C. Mangler, R. Drummond-Brydson, A. J. Scott, J. C. Meyer, J. Kotakoski, *2D Mater.* **2017**, *4*, 021013.

[67] P. A. Denis, *ChemPhysChem* **2014**, *15*, 3994.

[68] C. Rutherglen, D. Jain, P. Burke, *Nat. Nanotechnol.* **2009**, *4*, 811.

[69] F. Schwierz, *Nat. Nanotechnol.* **2010**, *5*, 487.

[70] S. Li, Z. Yu, S.-F. Yen, W. C. Tang, P. J. Burke, *Nano Lett.* **2004**, *4*, 753.

[71] G. De Angelis, A. Lucibello, E. Proietti, R. Marcelli, D. Pochesci, G. Bartolucci, M. Dragoman, D. Dragoman, *Nanomater. Nanotechnol.* **2011**, *1*, 64.

[72] G. Deligeorgis, M. Dragoman, D. Neculoiu, D. Dragoman, G. Konstantinidis, A. Cismaru, R. Plana, *Appl. Phys. Lett.* **2009**, *95*, 073107.

[73] M. Dragoman, D. Neculoiu, D. Dragoman, G. Deligeorgis, G.Konstantinidis, A. Cismaru, F. Coccetti, R. Plana, *IEEE Microwave Mag.* **2010**, *11*, 81.